Mechanical properties of epoxy composites reinforced using carbon fibers film-type coated with carboxyl graphene using a novel and economical electrophoretic deposition technique

Praveenkumar Jatothu[a], Alok K. Srivastava[a], Aparna Singh[b*]

[a] Centre for Research in Nanotechnology & Science, Indian Institute of Technology Bombay, Mumbai 400076, India

[b] Department of Metallurgical Engineering and Materials Science, Indian Institute of Technology Bombay, Mumbai 400076, India

Abstract

Carbon fiber reinforced polymer composites (CFRPs) show high specific strength and stiffness compared with other fiber reinforced polymer composites. However, these composites are most likely to fail at interface/interphase of fiber and epoxy owing to minimal interaction between the epoxy and the fiber due to the chemically inert nature of carbon fiber (CF) surface. Many CF surface modification techniques have been reported to increase the interfacial strength. Moreover, in some cases, incorporation of graphene fillers on CF surface is an effective way to enhance the interfacial adhesion strength between CF and epoxy. Electrophoretic deposition is an effective technique to deposit graphene nanofillers on CF fabric. In the current study, a novel combination of carboxyl functionalized graphene (G-COOH) and magnesium nitrate hexahydrate ($Mg(NO_3)_2.6H_2O$) has been chosen for preparing colloidal solution to deposit G-COOH on carbon fibers. This colloidal solution facilitates the adsorption of more Mg^{+2} ions on

*Corresponding author. E-mail address: aparna_s@iitb.ac.in (Aparna Singh), Tel: +91-22-2576-7605

the large number of active carboxyl functional groups present at the edges of G-COOH platelets and develops a positive charge on them. These platelets get deposited on cathodic electrode (i.e. carbon fiber fabric) with higher electrophoretic mobility during EPD. Hence, a uniform film-type layer of G-COOH platelets has been deposited with reduced EPD process parameters such as weight concentration of G-COOH platelets in suspension solution (g/L), deposition time and voltage compared to other studies. Surface morphology of G-COOH platelets deposition on carbon fiber fabric has been examined using scanning electron microscope (SEM). Surface characteristics of CFs has been studied using energy-dispersive X-ray spectroscopy (EDS) area mapping, FTIR and Raman spectroscopy. Four layers of pristine and G-COOH platelets deposited carbon fiber fabrics respectively have been used to manufacture the final composites through vacuum-assisted resin transfer molding (VARTM) technique. An increase in interphase thickness of G-COOH CF composite over pristine carbon fiber (PCF) composite was observed through carbon elemental EDS line scanning. G-COOH deposited CF composite showed enhancement in tensile strength and strain but reduction in flexural properties compared to PCF composites. This is due to higher prevalence of void formation in the G-COOH deposited composite.

Keywords: Carbon fiber, Carboxyl graphene, Electrophoretic deposition, VARTM, Strength

1. Introduction

Carbon fiber reinforced polymer composites (CFRPs) are commonly used in light weight high strength structural applications in various sectors such as aerospace, automobile, military, sports goods, marine, and civil etc. [1,2]. These composites exhibit high specific strength, stiffness as well as corrosion and wear resistance [3,4]. However,

the mechanically weakest link in CFRPs is generally the junction between the fiber and the epoxy due to weak bonding between them due to the chemically inert surface of CF [5]. The interface/interphase is a transition region where fiber and epoxy can potentially form chemical bonds and mechanical interlocking. Therefore, CFRPs' properties majorly depend on the interface/interphase strength of the transition region in which load transfer occurs from the epoxy to CF when subjected to mechanical loads [6].

Modification in interface/interphase through surface modification of CF using plasma treatment, oxidation treatment, sizing/coating modification, chemical deposition modification etc. has been reported by various researchers [7–11]. These methods enhance the surface roughness and chemical bond sites on CF to form mechanical interlocking and/or chemical bonding at the interface between epoxy and CF [6]. In recent years, graphene based nanofillers deposition has been increasingly attempted on CF owing to the former's high specific surface area, strength and stiffness compared to other carbonaceous nanofillers [12,13]. Moreover, many studies have been reported to enhance the mechanical properties of CFRPs through deposition of reduced graphene oxide (rGO) [14], amino-functionalized GO [15,16], graphene hydroxyl (G-OH) [17], graphene oxide (GO) [1,11,18–21] and graphene nanoplatelets (GNPs) [9,22] etc. on CF. Various deposition processes of graphene based nanofillers on CF are spray deposition [4,23], dip coating [24], chemical vapour deposition (CVD) [25] and electrophoretic deposition (EPD) [18,26–28] etc.

EPD has been found to be an effective deposition technique due to its exceptional capabilities such as uniform deposition, high efficiency and process parameters controllability [6]. EPD of graphene nanoplatelets involves two steps, electrophoresis and deposition. Electrophoresis is the movement of charged graphene platelets towards

the oppositely charged electrode in electric field and the subsequent accumulation of graphene platelets on opposite charged electrode is deposition [18].

Multiple studies have shown adsorption of the magnesium (Mg^{+2}) ions at edges of graphene nanosheets (GNS) owing to the presence of carboxyl functional groups during the dispersion of $Mg(NO_3)_2.6H_2O$/ $Mg(NO_3)_2$ and graphene sheets in a solution [29–31]. During EPD, dissociated ions of $Mg(NO_3)_2$ at the cathode can react with OH^- to generate $Mg(OH)_2$, which can support graphene nanosheets (GNS) on the substrate [29]. Moreover, lower voltage is preferential to magnesium (Mg^{+2}) ion-modified graphene nanosheets basal planes to align along the substrate [31]. Graphene (reduced or pure) is hydrophobic owing to the absence of functional groups. Many studies have been reported to functionalize graphene as graphene oxide (GO), and carboxyl graphene (G-COOH) [32]. Functional groups such as hydroxyl (-OH) and epoxide (C-O-C) are present on the basal plane of graphene, whereas the carboxyl (-COOH) group is present at the edges of the graphene structure. In carboxyl graphene, large number of carboxyl groups are present at the edges of graphene platelets and are highly reactive compared to other oxygen-based functional groups such as hydroxyl (-OH) and epoxide (C-O-C) etc [32].

Gangineni et al. reported a maximum improvement of 10% and 23% in flexural strength and inter laminar shear strength (ILSS) respectively of graphene carboxyl (G-COOH) coated CFRPs compared to other graphene nanofillers such as hydroxyl graphene (G-OH), graphene oxide (GO) and graphene (G). Surface morphology of EPD CF showed smooth (i.e. graphene surface wrapped to CF surface) and uniform deposition of G-COOH on a single CF surface. These graphene deposited carbon fiber fabrics were laminated through hand layup technique [33]. Yandrapu et al. studied the effect of EPD

process parameters on laminates made using the hand lay-up technique and reported an improvement of 26.6% and 35% in flexural strength and ILSS respectively of G-COOH coated CFRPs compared to uncoated CFRPs [27]. Surface morphology of EPD CF showed a few nanofillers along with a large quantity of adsorbed methyl violet (MV).

Surface morphology of previous studies on EPD could not achieve high density of G-COOH deposition onto the surface of CF fabric. Moreover, concentration of G-COOH in dispersion solution, current and time of deposition used in such studies were higher. Furthermore, the composites were fabricated using a hand-layup method. The optimization of EPD process parameters to minimize the time duration and nanofiller concentration has not been investigated so far. In addition, the combination of carboxyl functionalized graphene (G-COOH) and magnesium nitrate hexahydrate ($Mg(NO_3)_2.6H_2O$ has not been used for preparing EPD colloidal solution to deposit G-COOH on carbon fibers. Moreover, effect of uniform layer morphology of G-COOH on the extent of voids and the mechanical properties has not been investigated so far. Furthermore, manufacturing of such laminates through vacuum assisted resin transfer moulding (VARTM) technique has also not been explored. VARTM technique generally ensures high quality of the laminate in terms of high fiber volume fraction as well as low micro porosity/voids within the laminate. However, the mechanism of VARTM involves flow of the resin material, hence its effect on the quality of a graphene coated fiber reinforced laminate is not predictable.

In the current study, the interface between the carbon fiber and epoxy matrix has been modified through the coating of G-COOH nanoparticles on carbon fibers via novel colloidal solution for electrophoretic deposition technique. The G-COOH functionalized graphene has been dispersed in a solution containing $Mg(NO_3)_2 \cdot 6H_2O$ and DI water to

facilitate the larger adsorption of Mg^{+2} ions at the edges of carboxyl graphene. The presence of -COOH functional groups aims to increase the electrophoretic mobility of graphene in the dispersion during EPD. A uniform layer of G-COOH has been deposited on carbon fiber fabrics with a minimized time duration and nanofiller concentration during EPD. Further, G-COOH coated fabrics were used to manufacture the final laminates using VARTM technique and these laminates were tested under tensile and flexural loads. The morphology and characteristics of the pristine and G-COOH deposited carbon fibers has been examined through scanning electron microscopy (SEM), fourier-transform infrared spectroscopy (FTIR) and laser Raman spectroscopy. An optical stereo microscope was used to observe the delaminations and interply failure during the flexural test. Furthermore, failed specimens were examined under SEM to observe the failure mechanisms such as fiber-matrix debonding, fiber fracture and pull out etc.

2. Experimental

2.1 Materials

Carboxyl graphene (G-COOH) powder of average length and width ~5 – 10 μm, average thickness 5 – 10 nm, average no. of layers 5 – 10 and surface area 60 – 200 m^2/g was purchased from Techinstro, Maharashtra, India. Sizing coated polyacrylonitrile (PAN) based unidirectional carbon fibers (7 μm filament diameter) fabric of 200 gram per square meter (GSM) was procured from Bhor chemicals India Pvt. Ltd., Mumbai, India. Carbon fibers properties such as tensile strength (4000 MPa), density (1.8 g/cm^3) and percentage elongation (1.7%) were provided by the manufacturer's datasheet. DGEBA (Bisphenol–A–diglycidyl ether) based EPOFINE ®-5052 epoxy resin and FINEHARD ™- 5052 polyamine hardener were procured from

Fine Finish Organics Pvt. Ltd. Mumbai, India. The mixing ratio of epoxy resin and hardener 100:38 by-weight was given in manufacturer's datasheet. Extra pure magnesium nitrate hexahydrate ($Mg(NO_3)_2.6H_2O$) 98% was procured from Loba Chemie Pvt. Ltd. Mumbai, India. Except where otherwise specified, all materials were utilized exactly as they were received.

2.2 EPD solution preparation

A schematic representation of solution preparation used for the EPD process is shown in Fig. 1a. A concentration of 0.1 g/L of $Mg(NO_3)_2.6H_2O$ was dispersed in DI water and subsequently ultrasonicated for 15 minutes to homogenize the solution. Further, G-COOH platelets of concentration 0.1 g/L was added to the solution while doing ultrasonication for 5 minutes to obtain initial dispersion. Subsequently, suspension was probe sonicated for 45 minutes and ultrasonicated for 30 minutes to obtain a uniform dispersion of G-COOH. The prepared suspension was used in EPD process to coat G-COOH on the CF fabrics.

2.3 EPD process to deposit G-COOH on CF

A schematic representation of EPD process to deposit G-COOH on PCF fabrics is shown in Fig. 1b. First, unidirectional carbon fiber fabrics of 15 cm × 15 cm were covered with adhesive conductive copper tape along the edges of the fabrics to get a uniform electric field and structural stability during the deposition process. Then, these fabrics were immersed in prepared G-COOH and DI water suspension and connected to the cathode (-ve) as the working electrode. Further, two 15 cm × 15 cm stainless steel plates were immersed on either side of the fabrics with a 10 mm gap and connected to the anode (+ve) as counter electrodes. A constant direct current voltage of 15 V for 20 min was applied to the electrodes to deposit G-COOH platelets on the fabrics.

Simultaneously, ultrasonication was also done during the EPD process to get a uniform deposition throughout the fabric. Subsequently, wet deposited CF fabric was allowed to dry at room temperature for 2 hrs and in an oven at 80 ^{o}C for 8 hrs. After drying, the weight percent of deposited G-COOH on CF fabric was calculated by measuring the weight of CF fabric before and after EPD while weight of the copper tape was subtracted during calculation. The final weight percent of G-COOH deposited on CF via above mentioned EPD process parameters was found to be 1.3. Pristine and G-COOH coated carbon fiber fabrics were used to manufacture the final laminates.

2.4 Fabrication of G-COOH/CF/epoxy composites

A schematic representation of the VARTM method is shown in Fig. 1c. Vacuum bagging was done on a flat granite table after application of cleaner and mold releasing agent subsequently. Total four layers of carbon fiber fabric were stacked on the table in between the peel ply. Further, a flow mesh was used to stack on the top of the peel ply to ease the flow of the resin. Afterwards, a transparent bagging film was adhered on the table using a double-sided sealant tape and two openings were created using a high-pressure pipe for inlet and outlet of the resin. Meanwhile, epoxy resin and hardener were mixed manually in a ratio of 100:38 by-weight and the trapped air bubbles were subsequently removed by degassing it inside a vacuum chamber. At last, infusion of degassed epoxy and hardener mixture was performed through the inlet pipe by enabling the vacuum of 100 kPa via vacuum pump till complete infusion. Afterwards, vacuum was kept on for 24 hrs at ambient temperature after closing the inlet pipe and the prepared laminate was subsequently cured at 100^{o} C for 2 hrs. 1.3 wt.% G-COOH deposited carbon fibers fabric (1.3G-COOH CF) and pristine carbon fibers fabric (PCF) laminates were fabricated in similar steps.

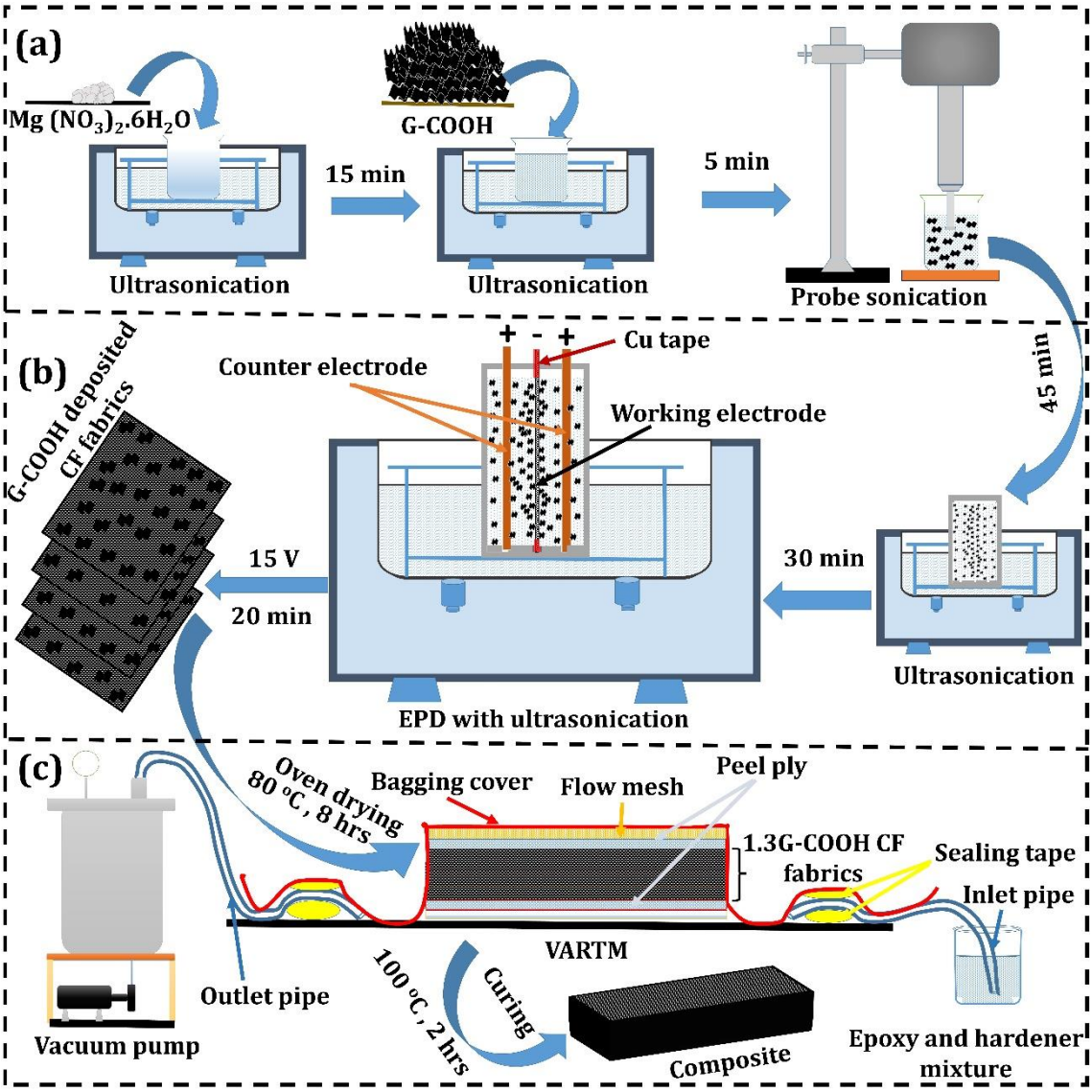

Fig. 1. Schematic representation of fabrication process of G-COOH/CF/epoxy composites (a) dispersion process of G-COOH, $Mg(NO_3)_2.6H_2O$ in DI water with ultrasonication and probe sonication, (b) deposition process of G-COOH on CF through EPD and (c) manufacturing of laminates through VARTM

2.5 Testing and characterization

Scanning electron microscope (SEM) (Hitachi S-3400 N) was used to observe the pristine and G-COOH deposited carbon fibers. As received G-COOH particles were also observed using SEM after drop casting them on a thin mica sheet. EDS line and area scanning was done on JEOL JSM-7600F field emission gun-scanning electron

microscopes (FEG-SEM) to obtain the elemental spectra. Cross sections of composites were polished with sand papers and Cr_2O_3 (100 nm particle size) powder-ethanol suspension subsequently before EDS line and area scanning under SEM. Fourier-transform infrared spectroscopy (FTIR) (Bruker, Germany-3000 Hyperion Microscope) was used to obtain the surface functional groups on G-COOH platelets and carbon fibers using powder-pressed KBr pallets. Wavelength range of 500 – 3500 cm^{-1} was taken with a spectra resolution of 0.2 cm^{-1}. Raman spectrometer (HORIBA HR 800) with 514.5 nm laser light was used to study the variation of graphitic structural disorder in G-COOH platelets and carbon fibers. Test was performed for 120 s at three different locations with 1 µm spot size and 20× magnification.

Tensile test was carried out on MTS hydraulic 100 kN capacity UTM machine. Dimension of tensile test CFRPs specimens was 10 mm (width), 1 mm (thickness) and 50 mm (gauge length). An extensometer of 25 mm length was used to record the strain during the test. A crosshead speed of 1 mm/min was used during the test and a minimum of three specimens of each condition were tested.

Universal testing machine (model: Instron E1000) of 1 kN capacity was used for three-point bend test. Specimens of dimensions 10 mm (width), 1 mm (thickness) and 40 mm (total length) were prepared for the test and a crosshead speed of 1 mm/min was used during the test. Minimum five specimens for each condition were tested and span to thickness ratio was taken as 30:1 as per ASTM D790. Optical images showing damage evolution during the flexural tests were extracted from the video recorded using a camera coupled with a stereo optical microscope.

3. Results

3.1 SEM micrographs of G-COOH platelets/PCF/1.3G-COOH CF

Fig. 2 shows the surface morphologies of as-received G-COOH platelets, PCF and 1.3G-COOH CF. Agglomerates and distinct few layered G-COOH platelets can be observed in Fig. 2a. In addition, various small platelets (indicated by yellow ovals) surrounding the large platelet in an order of nanoscale can be seen in Fig. 2b. A very neat and smooth surfaces of the pristine CFs are seen in Fig. 2c. However, longitudinal grooves are clearly visible in higher magnified micrograph of pristine CF (Fig. 2d). A layer of uniformly deposited G-COOH platelets on CF fabric can be observed in Fig. 2e. Nevertheless, few fibers deposited with individual platelets can be seen in Fig. 2f.

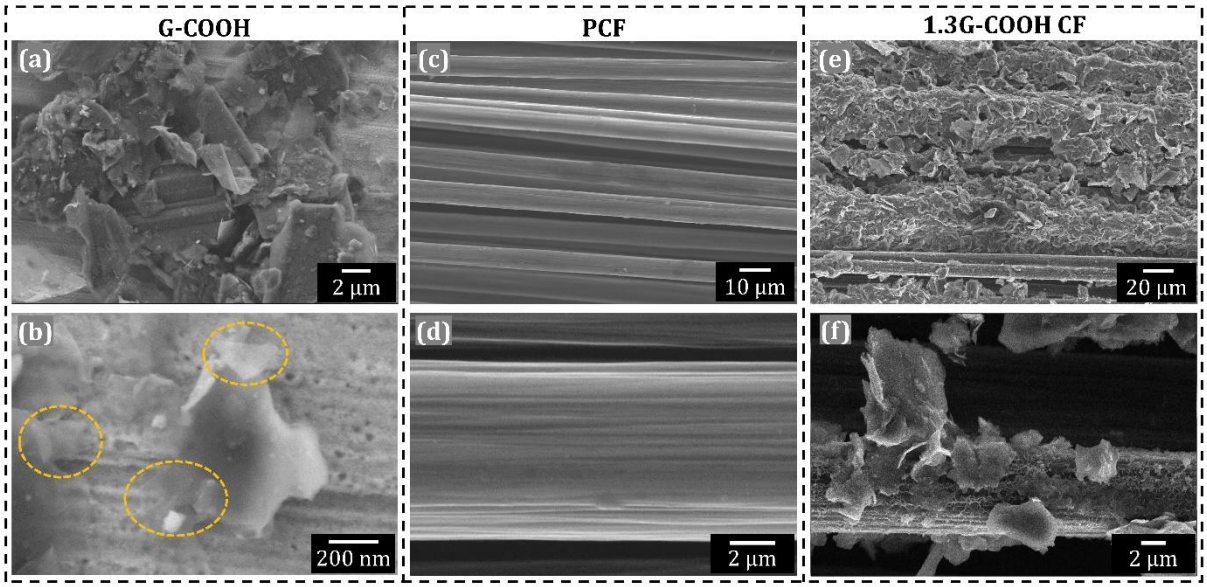

Fig. 2. SEM micrographs of (a, b) as-received G-COOH platelets, (c, d) PCF and (e, f) 1.3G-COOH CF

3.2 FTIR characteristics

FTIR spectra of G-COOH platelets, pristine CF and 1.3G-COOH CF has been recorded and the respective plots are shown in Fig. 3. Characteristic absorptions bands appear to be around 3433 cm^{-1} (–OH stretching vibrations), 2920 cm^{-1} (–CH stretching), 1724 cm^{-1} (C=O stretching vibrations) and 1056 cm^{-1} (C–O–C stretching vibrations) which are

indicative of hydroxyl, hydrocarbon, carbonyl, and epoxide functional groups respectively [28,34]. Moreover, peaks at 1629 cm^{-1} and 1228 cm^{-1} are indicative of C=C stretching vibrations and C–O bending vibrations respectively. The peaks of –OH and C=O confirms the presence of carboxylic functional group in G-COOH. The intensity of –OH on G-COOH deposited CF is found to be higher compared to pristine CF. Furthermore, C=C, C–O and C–O–C peaks of 1.3G-COOH CF are found to be slightly higher after EPD deposition.

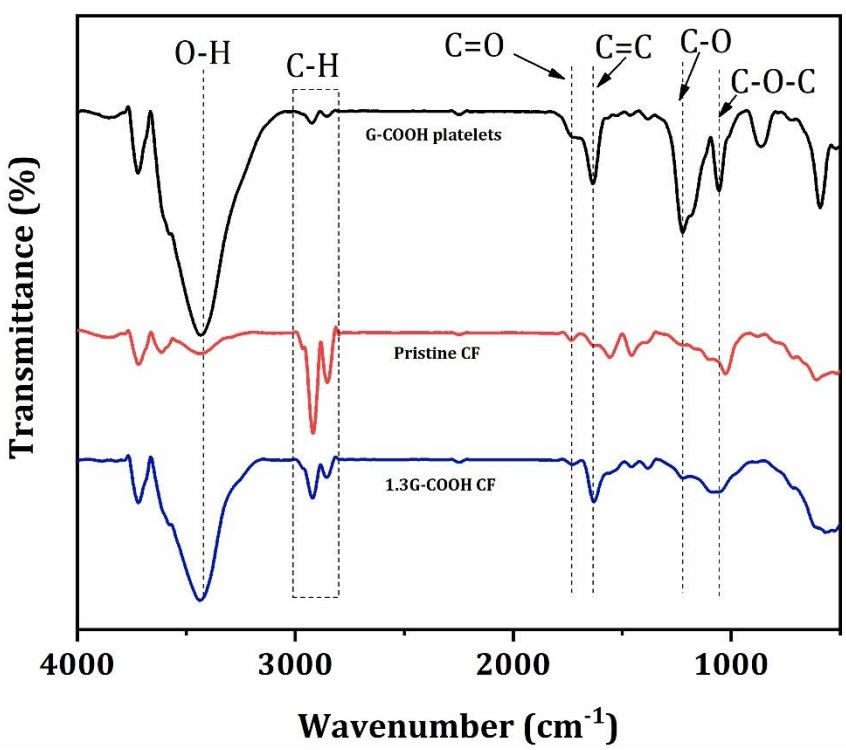

Fig. 3. FTIR spectra of G-COOH platelets, PCF and 1.3G-COOH CF

3.3 Raman characteristics

Fig. 4 shows the Raman spectra of G-COOH platelets, PCF and 1.3G-COOH CF. Primary in-plane vibrational mode of graphitic structure is represented by the G peak. The degree of disorder is represented by the D peak and the 2D peak. Second-order overtone of a distinct in-plane vibration is represented by 2D peak. The wavelengths of

1585 cm^{-1}, 1354 cm^{-1} and 2710 cm^{-1} indicate the G, D and 2D peaks respectively [31]. I_D/I_G and I_{2D}/I_G of G-COOH is 0.22 and 0.41 respectively which represents a low amount of disorder and a few layers of graphene (Fig. 4a). For pristine CF, the I_D/I_G ratio is higher (1.009) and no 2D peak has been seen (Fig. 4b). Deposition of G-COOH through EPD has resulted in a slightly higher I_D/I_G (1.079) in 1.3G-COOH CF compared to pristine CF. Increment in I_D/I_G might be due to the stacking disorder of deposited G-COOH platelets and conversion of sp^2 hybridized G-COOH platelets to sp^3 hybridization during EPD [35,36].

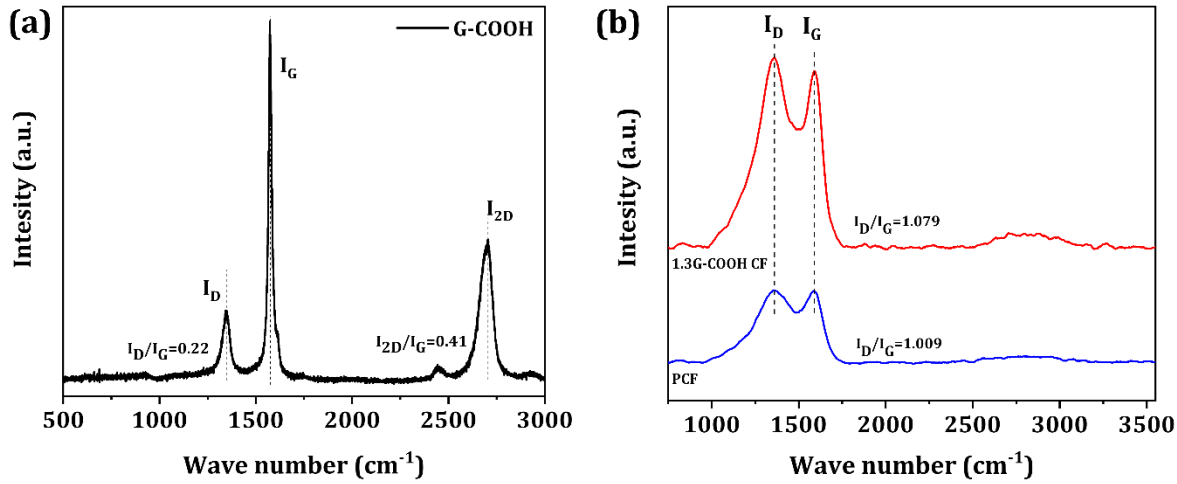

Fig. 4. Raman spectra of (a) G-COOH platelets (b) PCF and 1.3G-COOH CF

3.4 Interfacial characteristics of fiber

Fig. 5a and b show the SEM micrograph of transverse cross-section of the laminates along with EDS linear scanning plot. Representative images have been shown out of multiple images at different locations on the same specimen and the average interphase thickness was calculated for each laminate. Carbon fiber shows a higher intensity of carbon element, whereas, epoxy region shows comparatively less intensity of carbon element. The transition region which is also known as an interphase between CF and epoxy, shows a gradual reduction in carbon intensity from a higher to lower value.

Average interphase thickness of PCF and 1.3G-COOH CF laminates is 1.9 ± 0.5 μm and 2.9 ± 0.9 μm respectively which was obtained after averaging the values obtained at eight different locations on each laminate (Fig. 5c).

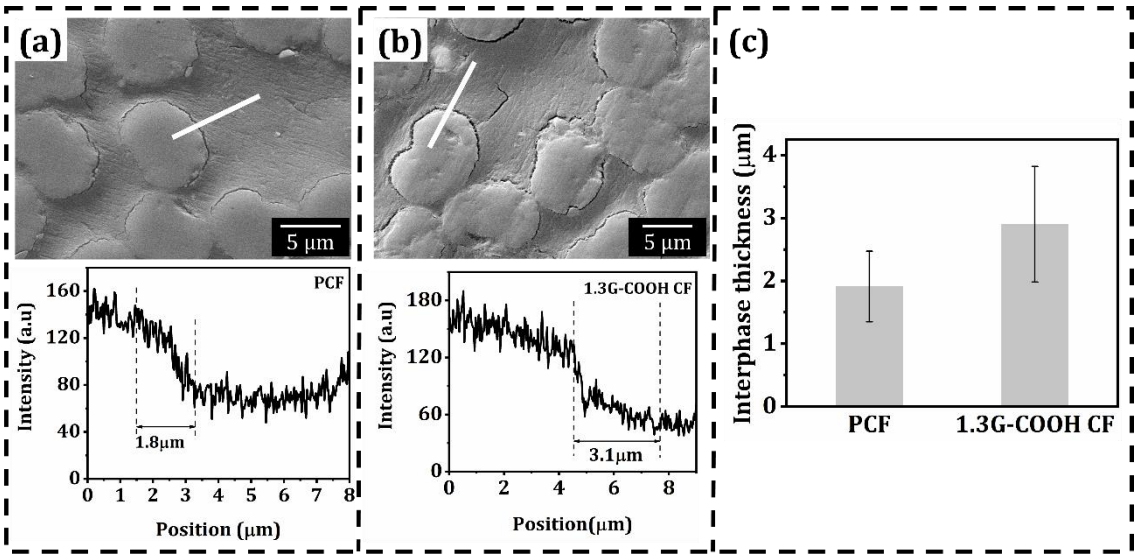

Fig. 5. SEM micrographs along with carbon elemental EDS line scan plot of (a) PCF and (b) 1.3G-COOH CF composite; (c) average interphase thickness of PCF and 1.3G-COOH CF composites

3.5 Tensile characteristics of PCF/ 1.3G-COOH CF composite

Fig. 6(a) shows the representative stress vs. strain curves for PCF and 1.3G-COOH CF composite tested under uniaxial tension along the longitudinal direction of CFs. Average tensile properties such as tensile strength and modulus, strain at maximum tensile stress for both composites are shown in Fig. 6 b and c. Three specimen's average data for each laminate is shown in Table 1. It is observed that there is an improvement of 25% and 30% in tensile strength and strain at failure respectively of 1.3G-COOH CF composite compared to PCF composite (Fig. 6a-b).

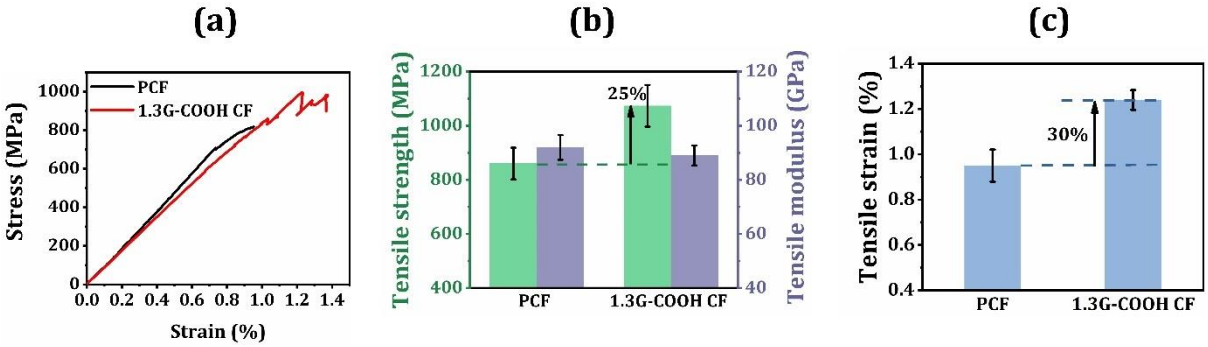

Fig. 6. Tensile properties of PCF and 1.3G-COOH CF composites (a) stress vs. strain curves (b) tensile strength and modulus (c) strain at maximum tensile stress

Table 1. Tensile properties of PCF and 1.3G-COOH CF composites

Specimen	***Tensile strength (MPa)***	***Tensile modulus (GPa)***	***Strain at maximum tensile stress (%)***
PCF	860 ± 58	92 ± 1.7	0.95 ± 0.07
1.3G-COOH CF	1073 ± 77	89 ± 2.7	1.24 ± 0.04

Fig. 7 shows the SEM micrographs of fractured surfaces of PCF and 1.3G-COOH CF composites tested under uniaxial tension. Transverse fractured surfaces of PCF composites show debonding gaps at the fiber-epoxy interface (Fig. 7a). Whereas, failure at the interphase region, and adhered epoxy/G-COOH along with G-COOH platelets can be observed in 1.3G-COOH CF composites (Fig. 7c). Fracture surface of PCF composite in longitudinal direction shows a thin broken layer of epoxy in between the fibers (indicated by red oval in Fig. 7b). Neat fibers, straight crack propagation and thick layers of failed epoxy can also be seen on/between the carbon fibers (indicated by red, black and yellow arrows respectively in Fig. 7b). Longitudinal fractured surface of 1.3G-COOH CF composite shows the complete adherence of G-COOH mixed epoxy on the fibers (Fig. 7d). Further, fiber imprints as well as minor cracks/deflected crack

propagation on the layer of G-COOH mixed epoxy can be seen in Fig. 7d which represents crack deflection happening to avoid hitting graphene particles.

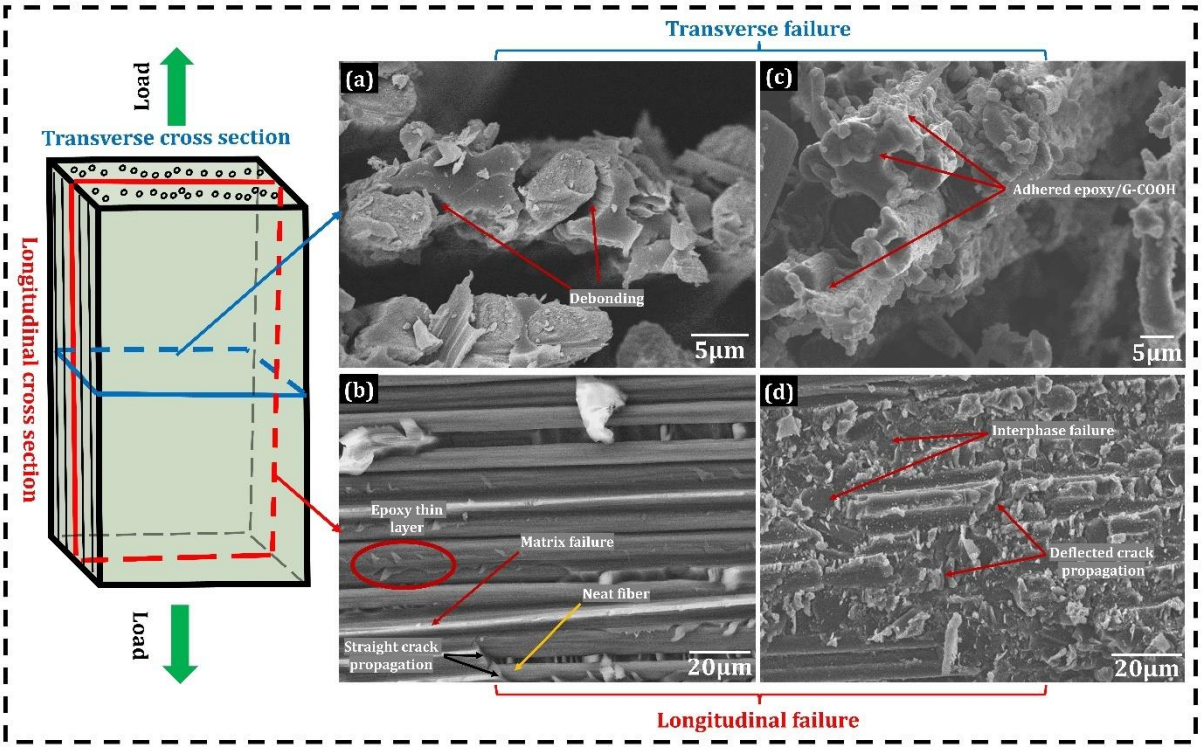

Fig. 7. SEM micrographs of transverse and longitudinal fractured surfaces of (a, b) PCF composite and (c, d) 1.3G-COOH CF composites tested under uniaxial tensile loads

3.6 Flexural characteristics of PCF/ 1.3G-COOH CF composite

Flexural properties of PCF and 1.3G-COOH CF composites have been plotted in Fig. 8. The average of three specimen's data for each laminate has been shown in Table 2. A reduction of 51%, 27%, and 11% in flexural strength, strain, and modulus respectively of 1.3G-COOH CF composites has been observed compared to PCF composites (Fig. 8a-b).

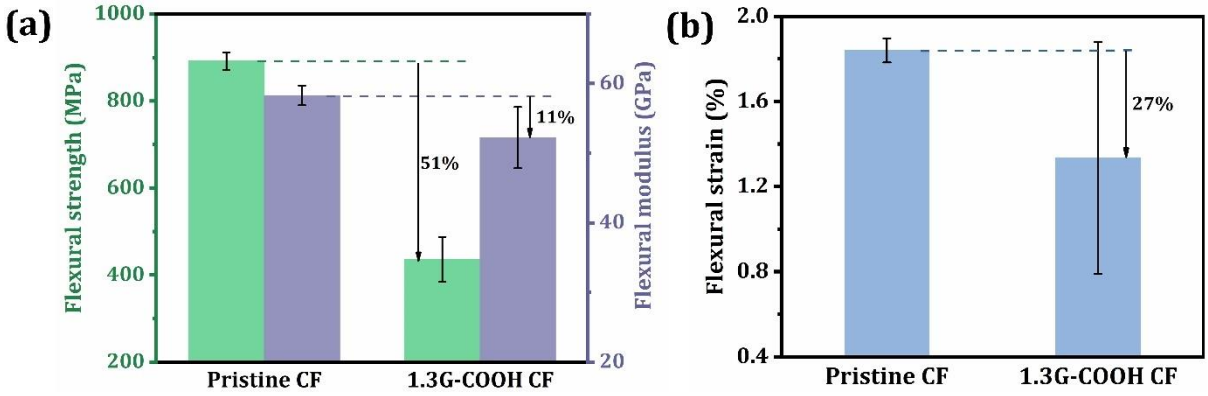

Fig. 8. Flexural properties of PCF and 1.3G-COOH CF composites (a) flexural strength and modulus (b) strain at maximum flexural stress

Table 2. Flexural properties of PCF and 1.3G-COOH CF composites

Specimen	***Flexural strength (MPa)***	***Flexural modulus (GPa)***	***Strain at maximum flexural stress (%)***
PCF	892 ± 20	53 ± 0.4	1.84 ± 0.05
1.3G-COOH CF	436 ± 51	47 ± 3.5	1.33 ± 0.5

Fig. 9 shows the flexural test in-situ optical images along with stress v/s strain graph for PCF and 1.3G-COOH CF composites. PCF composite shows a continuous increment of flexural stress that can be observed from point 1 to 2 and reduction in load has occurred at point 2 (Fig. 9a). The stress increases further till point 3 with reduced modulus and reaches its maximum value. Subsequently top layer initial failure has been observed away from the centre (indicated by yellow oval in Fig. 9a-4) along with a sudden load drop till point 4. Subsequently, delamination somewhere near the neutral axis of the composite starts and is connected with crack propagating till the bottom of the composite. (Fig. 9a-5 & 5').

Longitudinal cross section of 1.3G-COOH CF composite shows voids (indicated by white arrows in Fig. 9b-1) at multiple locations, which were not present in PCF composite. A continuous increment in stress has been observed from point 1 to 2 in 1.3G-COOH CF composite. Later, a kink band (indicated by yellow oval in Fig. 9b-2) has been initiated at void region in top layer of composite. This kink band has grown along with initiation of another kink band at a different location (indicated by yellow ovals in Fig. 9b-3) till location 3 with reduced modulus. Subsequently, a new crack has initiated from the void region below the loading ram which propagated to top surface of composite (Fig. 9b-4) with a sudden load drop till location 4. Further, previous crack has been arrested while the load has increased till the maximum at point 5 with reduced modulus (Fig. 9b-5). After that, same crack has propagated towards the bottom ply with a gradual reduction in load and the bottom ply did not fail till point 6 (Fig. 9b-6, 6').

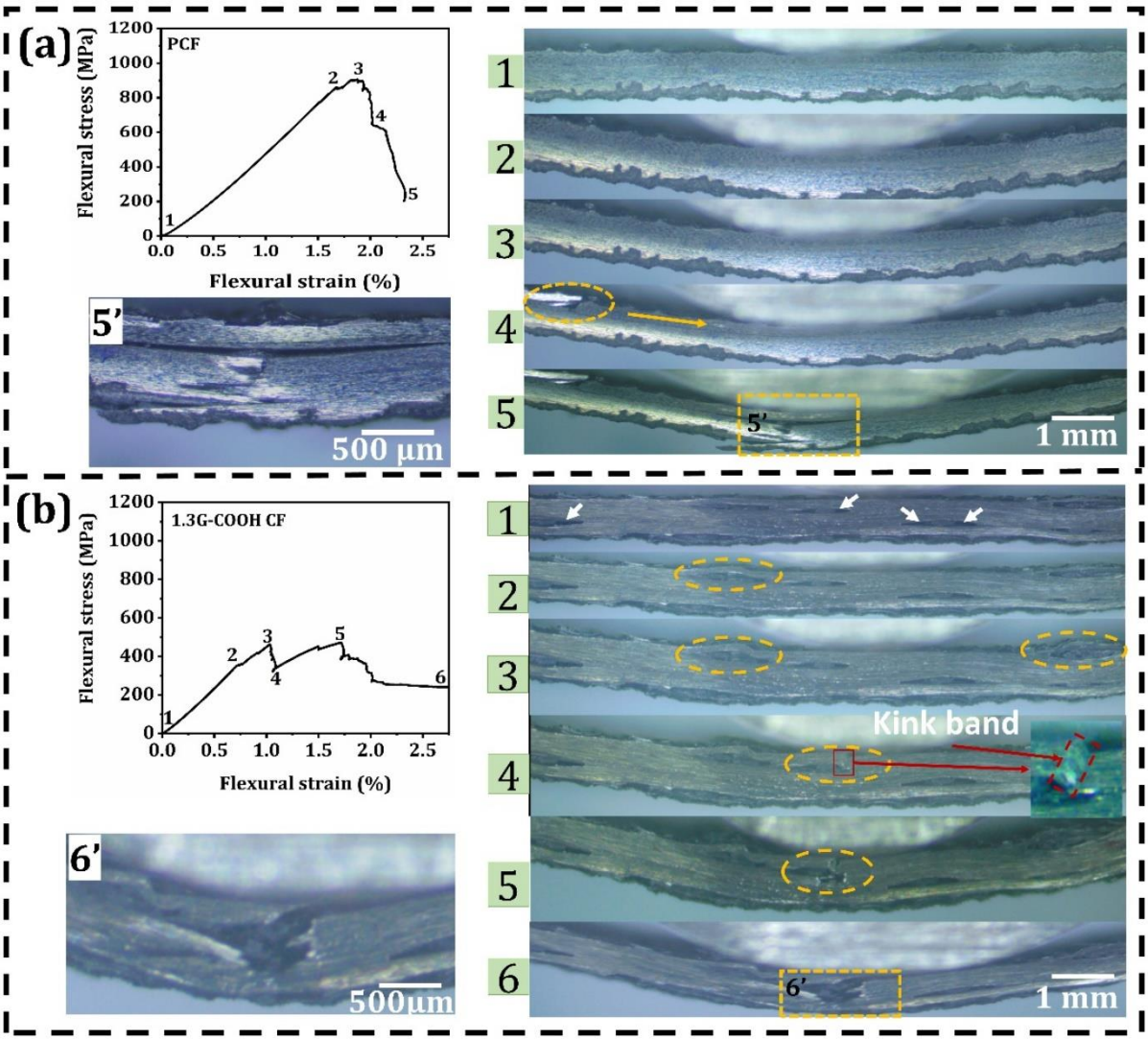

Fig. 9. In-situ flexural test optical images w.r.t to appropriate instant in stress v/s strain graph of (a) PCF and (b) 1.3G-COOH CF composites

Fig. 10 shows the SEM micrographs of the transverse fracture surfaces for pristine and 1.3G-COOH CF laminates which were tested under flexural loads. Both laminate's fracture surfaces showed three different regions in Fig. 10 (A) & (B); (a) compression under the loading ram, (b) transition region and (c) tensile region. Particles of epoxy at the compression region on the fracture surface of both the laminates can be seen in Fig. 10 (A-a, B-a). Fiber failure with some angle w.r.t to the longitudinal direction of fiber can be seen in pristine laminate (Fig. 10 A-a). However, the presence of a large amount

of graphene/epoxy debris are seen on the fracture surface of 1.3G-COOH CF laminate (Fig. 10 B-a). There is a transition region near to the middle layer of both the laminates which can be seen in Fig. 10 (A-b, B-b). In pristine laminate (Fig. 10 (A-b), the transition from compressive to tensile region is fairly smooth which is noticeable through the presence of small amount of epoxy debris in compressive region and clean broken fiber surfaces in tension region.). Many fiber pull-outs and fiber-epoxy debonded regions have been observed in pristine laminates (Fig. 10 A-c'). A large number of clean broken fibers are seen in tensile region of pristine laminates Fig. 10 A-c). However, transition region in 1.3G-COOH CF composite shows a dense fiber fracture in compression and a few fiber failures along with fiber pull out in tensile regions (Fig. 10B-b). However, aadhered epoxy/G-COOH and a few fiber pullouts can be observed in tensile failure region of 1.3G-COOH CF composites (Fig. 10B-c-c').

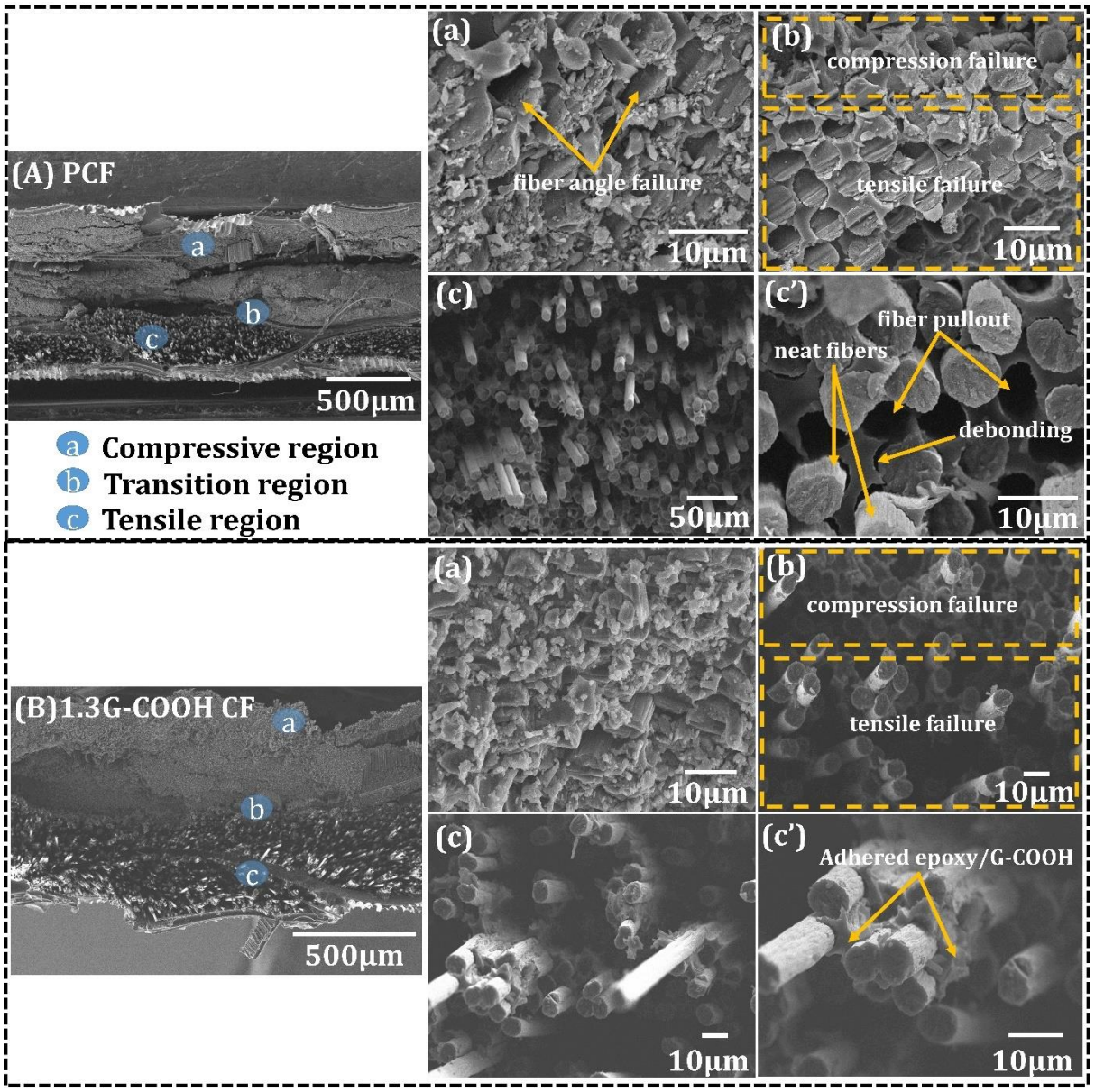

Fig. 10. SEM micrographs of fractured surfaces of (A) PCF and (B) 1.3G-COOH CF composites tested under flexural load

4. Discussion

A novel homogeneous colloidal solution was prepared for the EPD process by dispersing $Mg(NO_3)_2.6H_2O$ and G-COOH in DI water to deposit a uniform thin layer of G-COOH platelets on CF fabrics. The carboxyl functional groups (-COOH) that are present at the edge of G-COOH platelets are capable of adsorbing magnesium positive ions in an aqueous solution [32]. Consequently, G-COOH platelets become positively

charged during ultrasonic dispersion. These G-COOH platelets could exhibit mutual repulsion when they come into close proximity, preventing agglomeration in the dispersion solution and resulting in increased electrophoretic mobility during EPD. As a result, thin uniform film-type deposition of G-COOH platelets happened on CF fabric during EPD (Fig. 2e-f). Moreover, the rate of EPD depends on the quantity of surface charge present on graphene nanoparticles [18,37] which is large due to -COOH groups at the edge of G-COOH platelets having absorbed significantly higher magnesium positive ions. Thus, a uniform thin layer of G-COOH platelets deposition was achieved with minimal EPD process parameters such as G-COOH dispersion concentration (0.1 g/L), Voltage (15 V), time (20 min), the gap between electrodes (1 mm) compared to other studies [27,33].

The weight percentage of a thin layer of G-COOH platelets deposited on PCF fabric was obtained as 1.3 wt.% which led to the development of larger interphase thickness in 1.3G-COOH CF composites compared to PCF composites (shown in Fig. 5 and Fig. 11a). Improved tensile strength of 1.3G-COOH CF composite might be attributed to the formation of a larger interphase, chemical bonding, and mechanical interlocking among CF, G-COOH and epoxy. Jiang et al. have shown that the adhesion between carbon fiber and epoxy increases through hydrogen bond formation between oxygen-based functional groups and epoxy [19]. 1.3G-COOH CF composites have shown larger tensile failure strain compared to PCF composites which might be attributed to the presence of G-COOH platelets in the interphase region. G-COOH particles hinder the crack which starts from the epoxy and propagates towards the CF surface. The larger interphase region could transfer load uniformly by keeping stress concentration away from the CF surface through the transition of modulus between fiber and epoxy.

Schematic of failure mechanisms of the fiber/epoxy/G-COOH junction of PCF and 1.3G-COOH CF composites under uniaxial tension has been shown in Fig. 11b and c. Longitudinal failure of PCF composites can be attributed to straight crack propagation from epoxy region to the CF surface as the interphase is not able to effectively deviate the crack (Fig. 11b and Fig. 7b). However, the presence of G-COOH in the interphase region of 1.3G-COOH CF composites results in crack deflection leading to a tortuous crack path through the interphase (Fig. 11 and Fig. 7d). Moreover, transverse failure of PCF composites reveals debonding gaps between CF and epoxy which might be due to poor interfacial bonding (Fig. 7a). Whereas, presence of adhered epoxy/G-COOH on carbon fibers confirms the increased interfacial bonding in 1.3G-COOH CF composites (Fig. 11c and Fig. 7c).

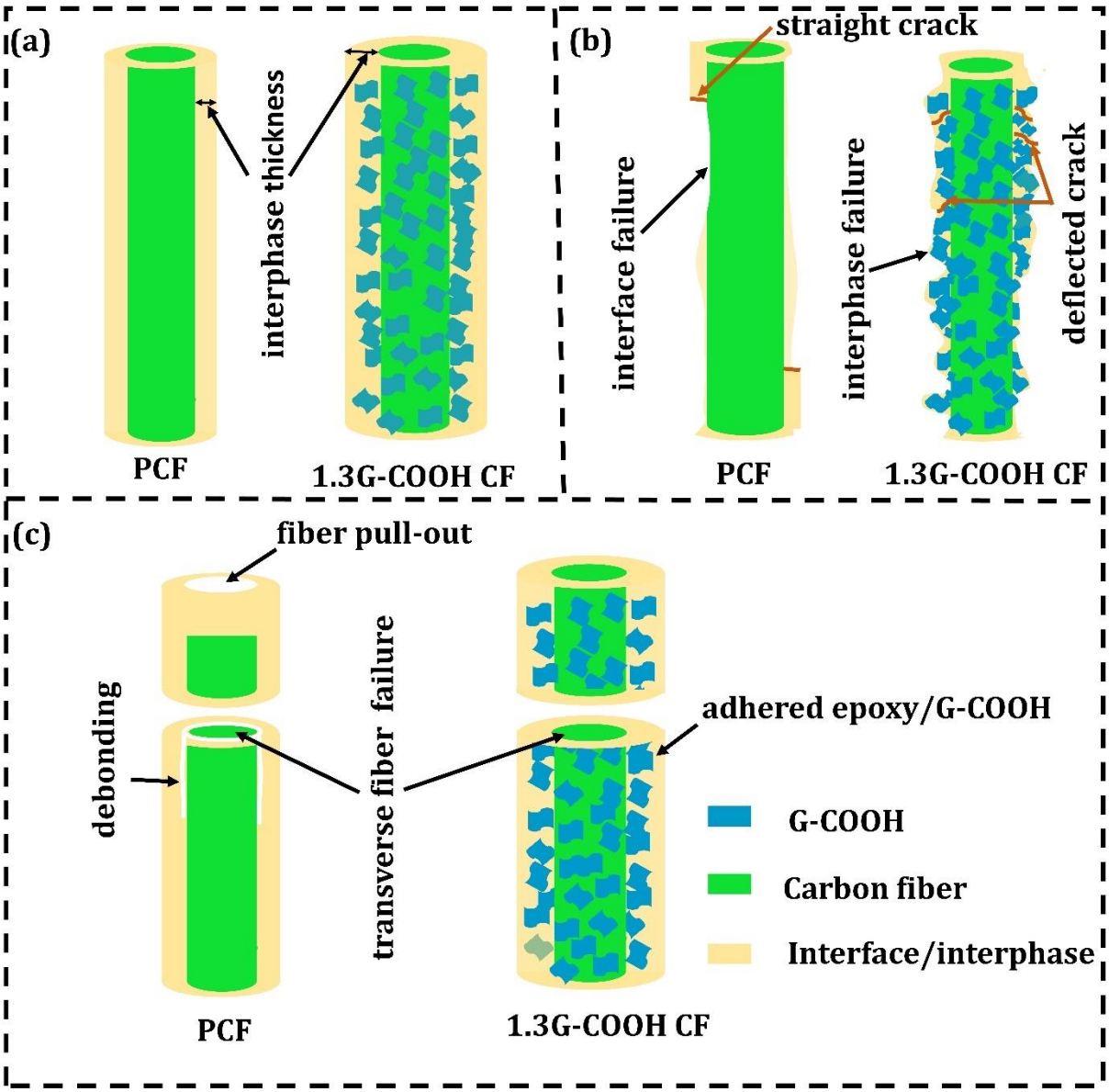

Fig. 11. Schematic representation of G-COOH/epoxy/fiber junction of PCF and 1.3G-COOH CF composites (a) undeformed laminate showing interphase thickness; (b) longitudinal and (c) transverse fracture when subjected to tensile loading

Flexural properties of 1.3G-COOH CF composite such as strength, modulus, and strain are found to be decreased compared to PCF composite (Fig. 8). This decrease in strength can be attributed to the presence of voids (Fig. 12), which prevent neighboring fibers from fully bonding with the epoxy. This results in weak areas that cannot withstand applied loads, ultimately leading to failure initiation from these regions. Load

transfer efficiency from epoxy to fiber depends on the chemical bond between epoxy and nanofiller whereas mechanical interlocking depends on infiltration [33]. According to infiltration theory, interfacial enhancement is possible with good wettability and void-free surface of CF [38]. Resin-starving regions or voids at the interface of CF show an adverse effect on the load-carrying capabilities of composite [14]. The presence of voids in the 1.3G-COOH CF composite may be attributed to the deposition of a thin layer of G-COOH platelet on the PCF fabric, which resulted in inadequate impregnation of epoxy during fabrication. The deposition of G-COOH in film form can obstruct and reduce the velocity of resin flow between fabric layers (i.e. macroscopic flow), causing it to be slower compared to the flow between individual fibers within the fabric tows (i.e. microscopic flow). As a consequence, air can be trapped between the fabric layers due to the merging of the microscopic flow in front of macroscopic flow, resulting in the formation of voids with an elliptical cross-sections [39]. The schematics representation of the resin flow during the fabrication of these composites can be seen in Fig. 13.

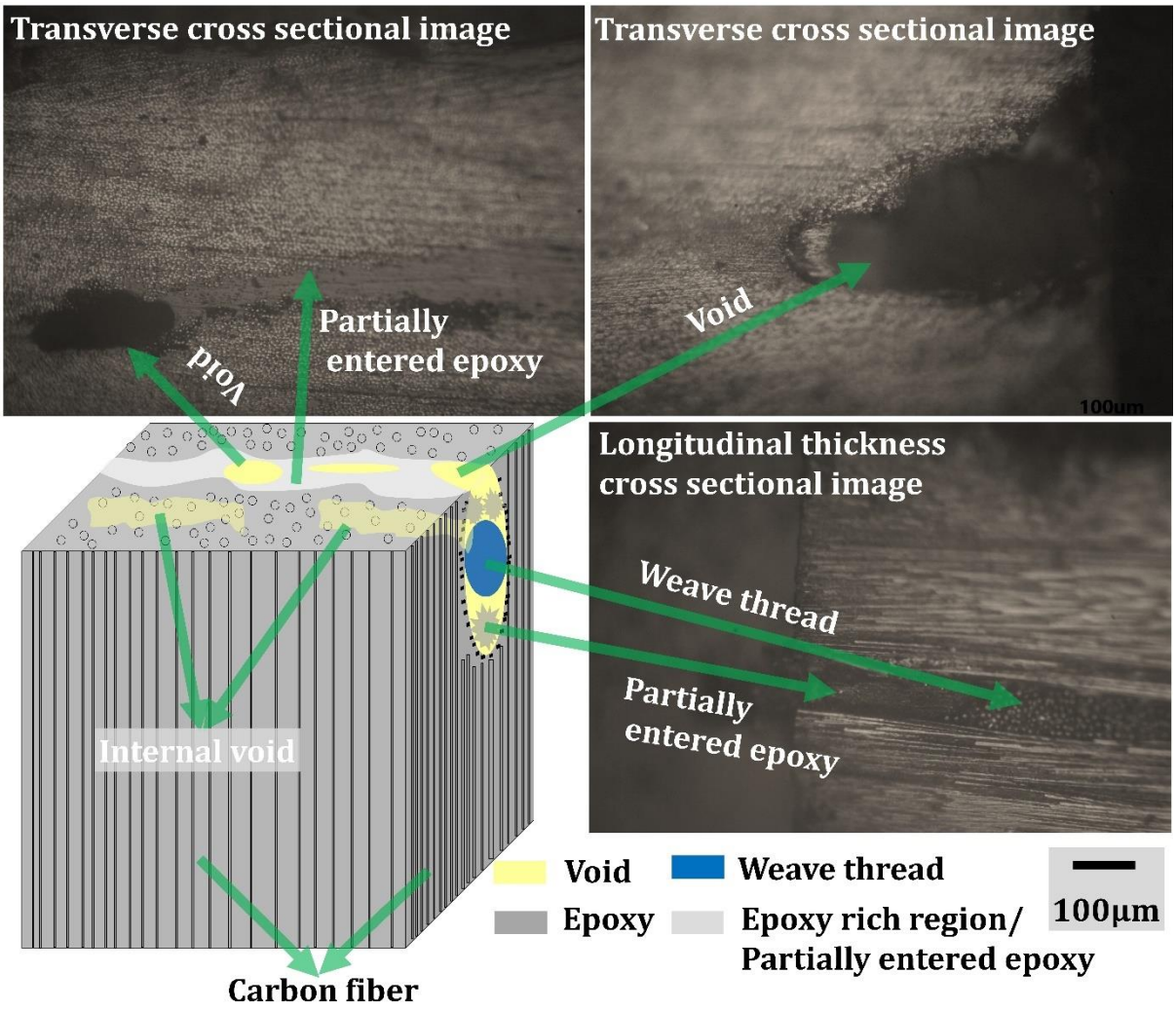

Fig. 12. Schematics of voids in 1.3G-COOH CF composite along with optical micrographs of transverse and longitudinal thickness section

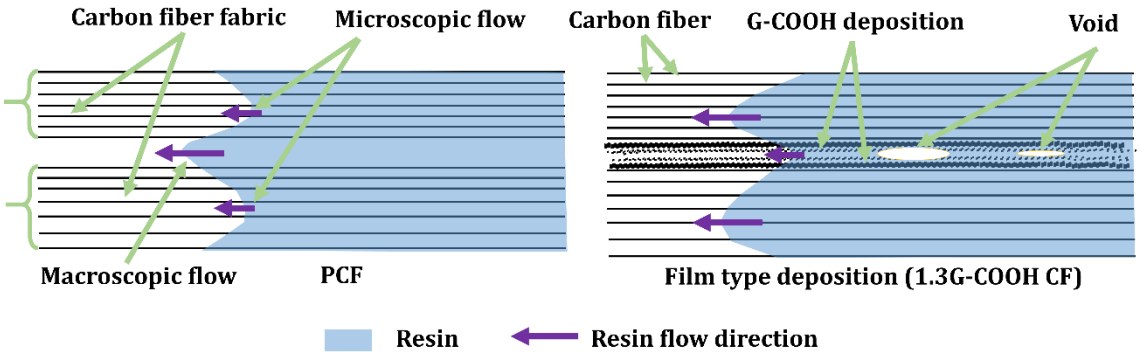

Fig. 13. Schematic representation of the resin flow during the fabrication of PCF and 1.3G-COOH CF composites

Flexural failure in 1.3G-COOH CF composite initiated through formation of kink bands (Fig. 9b-4) at the void regions, which resulted in a decrease in load capacity. However, further increase in load was attributed to the load bearing capacity of the remaining plies, ultimately leading to the progressive failure of the composite while the bottom plies of the specimen's remain intact at higher strains compared to pristine composites. In addition, brittle crushing of epoxy (Fig. 9b-5) might be result of gradual load transfer from epoxy to fiber through larger interphase. On the other hand, failure of the PCF composite initiated through the ply failure at the top (Fig. 9a-4), propagated with sudden load drop, showing major delamination and rapid plies failure through the thickness along with delamination due to weak interface strength between CF and epoxy. The final fracture of the PCF composites showed transverse ply failure till the bottom-most ply at a smaller flexural strain compared to 1.3G-COOH CF composite, which could be the result of crack deflection at interphase region/voids of 1.3G-COOH CF. Neat fibers, debonding between fiber and epoxy, and large fiber pull out in PCF composites have been attributed to the poor interfacial interaction and weak interfacial strength between fiber and epoxy (Fig. 10A-c-c'). However, the lesser number of fiber pullouts in 1.3G-COOH CF composite could be due to mechanical interlocking (i.e. friction between the fiber and G-COOH) of epoxy along with G-COOH in the groove/furrows of CF [39].

G-COOH coating of 1.3 wt.% through EPD process resulted in enhancement of tensile properties such as strength and strain at maximum load, while flexural properties of these composites deteriorated. This contrast might be attributed to presence of voids in 1.3G-COOH CF composites. Most of the voids in the 1.3G-COOH CF composite are oriented along the fiber direction and hence the tensile properties are not deteriorated but enhanced due to the presence of the G-COOH. However, for flexural loading, the

voids located in the compression region may expand in the transverse direction, leading to the formation of kink bands. This effect seems to be dominant over interphase strengthening through G-COOH.

5. Conclusions

The present study involves altering the interface between carbon fibers and epoxy matrix by applying a novel colloidal solution for electrophoretic deposition technique to coat G-COOH nanoparticles onto the carbon fibers. A combination of carboxyl functionalized graphene (G-COOH) and magnesium nitrate hexahydrate has been used in cathodic EPD to deposit G-COOH on carbon fibers. A set of optimized EPD process parameters such as such as 15 V voltage, 20 min time and 0.1 g/L G-COOH was used for thin layer of G-COOH platelets (1.3 wt.%) of deposition. Moreover, the ratio of magnesium nitrate hexahydrate and G-COOH platelets used was 1:1 for this type of deposition morphology and the concentration of G-COOH required was much less than other studies. 1.3G-COOH CF and PCF fabrics of four layers were used for fabrication of composites through VARTM technique. The major outcomes of the current study are as follows:

- A uniform thin layer of G-COOH deposited through EPD has resulted in the formation of a larger interphase in G-COOH composites compared to PCF composites.
- G-COOH composite showed a significant improvement in tensile strength, and strain at maximum stress as compared to pristine carbon fiber composite which might be primarily attributed to the enhanced interphase strength due to film-type G-COOH deposition on CF.

- SEM fractographs of longitudinal and transverse views of fracture surfaces of pristine carbon fiber composite revealed the presence of neat carbon fibers, thin layers of epoxy and debonding gaps between fibers respectively. However, similar views of fracture surfaces of G-COOH deposited composite showed the presence of thick layer of G-COOH/epoxy due to interphase failure and adherence of epoxy/G-COOH on carbon fibers.
- Voids were seen in composites reinforced with G-COOH deposited composites due to difficulty in resin flow due to restricted flow channel between fabric layers after deposition of film-type G-COOH.
- Composites reinforced with G-COOH-deposited carbon fibers exhibited reduced flexural strength compared to the pristine carbon fiber composites. The primary reason for this decline was delamination caused by the presence of voids (resin-starved regions) in G-COOH-deposited composites. Consequently, the void formation played a more significant role than the influence of interphase strength enhancement in determining the flexural properties of the film-type G-COOH-deposited composites.

Declarations of interest

Authors have filed a patent (Indian patent application no. – 202321028884) for achieving a uniform film-type deposition on carbon fiber fabric which is under examination. All authors declare that they have no other conflicts.

REFERENCES

[1] Sharma H, Kumar A, Rana S, Guadagno L. An Overview on Carbon Fiber-Reinforced Epoxy Composites: Effect of Graphene Oxide Incorporation on Composites Performance. Polymers (Basel) 2022;14.

https://doi.org/10.3390/polym14081548.

[2] Sayam A, Rahman ANMM, Rahman MS, Smriti SA, Ahmed F, Rabbi MF, et al. A review on carbon fiber-reinforced hierarchical composites: mechanical performance, manufacturing process, structural applications and allied challenges. vol. 32. Springer Nature Singapore; 2022. https://doi.org/10.1007/s42823-022-00358-2.

[3] Srivastava AK, Desai U, Singh A. Effect of graphene coating on modified and pristine carbon fibers on the tribological response of carbon fiber epoxy composites. Compos Part B Eng 2023;250:110412. https://doi.org/10.1016/j.compositesb.2022.110412.

[4] Srivastava AK, Singh A. Effect of Graphene Coating of Carbon Fibers on the Fracture of Uni-directional Laminates. Procedia Struct Integr 2022;41:241–7. https://doi.org/10.1016/j.prostr.2022.05.027.

[5] Liu F, Wang D, Liu J, Wei H, Zhang H, Xu J, et al. Reviews on Interfacial Properties of the Carbon Fiber Reinforced Polymer Composites. J Phys Conf Ser 2020;1637. https://doi.org/10.1088/1742-6596/1637/1/012027.

[6] Zheng H, Zhang W, Li B, Zhu J, Wang C, Song G, et al. Recent advances of interphases in carbon fiber-reinforced polymer composites: A review. Compos Part B Eng 2022;233:109639. https://doi.org/10.1016/j.compositesb.2022.109639.

[7] Xie J, Xin D, Cao H, Wang C, Zhao Y, Yao L, et al. Improving carbon fiber adhesion to polyimide with atmospheric pressure plasma treatment. Surf Coatings Technol 2011;206:191–201. https://doi.org/10.1016/j.surfcoat.2011.04.016.

[8] Lee E seok, Lee C hyun, Chun YS, Han C ji, Lim DS. Effect of hydrogen plasma-mediated surface modification of carbon fibers on the mechanical properties of carbon-fiber-reinforced polyetherimide composites. Compos Part B Eng 2017;116:451–8. https://doi.org/10.1016/j.compositesb.2016.10.088.

[9] Srivastava AK, Gupta V, Yerramalli CS, Singh A. Flexural strength enhancement in carbon-fiber epoxy composites through graphene nano-platelets coating on

fibers. Compos Part B Eng 2019;179:107539. https://doi.org/10.1016/j.compositesb.2019.107539.

[10] Srivastava AK, Gupta V, Yerramalli CS, Singh A. Mechanical properties of graphene nano-platelets coated carbon fiber epoxy composites. ICCM Int. Conf. Compos. Mater., vol. 2019- Augus, Engineers Australia; 2019, p. 163–71.

[11] Wang C, Li J, Sun S, Li X, Zhao F, Jiang B, et al. Electrophoretic deposition of graphene oxide on continuous carbon fibers for reinforcement of both tensile and interfacial strength. Compos Sci Technol 2016;135:46–53. https://doi.org/10.1016/j.compscitech.2016.07.009.

[12] Chavez-Valdez A, Shaffer MSP, Boccaccini AR. Applications of graphene electrophoretic deposition. A review. J Phys Chem B 2013;117:1502–15. https://doi.org/10.1021/jp3064917.

[13] Geim AK and KSN. 2007_the rise of graphene.pdf 2007:183–91.

[14] Bhanuprakash L, Parasuram S, Varghese S. Experimental investigation on graphene oxides coated carbon fibre/epoxy hybrid composites: Mechanical and electrical properties. Compos Sci Technol 2019;179:134–44. https://doi.org/10.1016/j.compscitech.2019.04.034.

[15] Sun T, Zhang X, Qiu B, Zhang H, Yan L, Liang M, et al. Electrochemical construction of amino-functionalized GO/carbon fiber multiscale structure to improve the interfacial properties of epoxy composites. Mater Chem Phys 2022;286:126197. https://doi.org/10.1016/j.matchemphys.2022.126197.

[16] Deng C, Jiang J, Liu F, Fang L, Wang J, Li D, et al. Effects of electrophoretically deposited graphene oxide coatings on interfacial properties of carbon fiber composite. J Mater Sci 2015;50:5886–92. https://doi.org/10.1007/s10853-015-9138-2.

[17] Patnaik S, Gangineni PK, Ray BC, Prusty RK. Effect of graphene-based nanofillers addition on the interlaminar performance of CFRP composites: An assessment of cryo-conditioning. Mater Today Proc 2020;33:5070–5. https://doi.org/10.1016/j.matpr.2020.02.846.

[18] Ma Y, Han J, Wang M, Chen X, Jia S. Electrophoretic deposition of graphene-based materials: A review of materials and their applications. J Mater 2018;4:108–20. https://doi.org/10.1016/j.jmat.2018.02.004.

[19] Jiang J, Yao X, Xu C, Su Y, Deng C, Liu F, et al. Preparation of Graphene Oxide Coatings onto Carbon Fibers by Electrophoretic Deposition for Enhancing Interfacial Strength in Carbon Fiber Composites. J Electrochem Soc 2016;163:D133–9. https://doi.org/10.1149/2.0571605jes.

[20] Hung P yan, Lau K tak, Fox B, Hameed N, Jia B, Lee JH. Effect of graphene oxide concentration on flexural properties of CFRP at low temperature. Carbon N Y 2019;152:556–64. https://doi.org/10.1016/j.carbon.2019.06.032.

[21] Zhang X, Fan X, Yan C, Li H, Zhu Y, Li X, et al. Interfacial microstructure and properties of carbon fiber composites modified with graphene oxide. ACS Appl Mater Interfaces 2012;4:1543–52. https://doi.org/10.1021/am201757v.

[22] Awan FS, Fakhar MA, Khan LA, Subhani T. Study of Interfacial Properties of Carbon Fiber Epoxy Matrix Composites Containing Graphene Nanoplatelets. Fibers Polym 2019;20:633–41. https://doi.org/10.1007/s12221-019-8596-6.

[23] Wang F, Cai X. Improvement of mechanical properties and thermal conductivity of carbon fiber laminated composites through depositing graphene nanoplatelets on fibers. J Mater Sci 2019;54:3847–62. https://doi.org/10.1007/s10853-018-3097-3.

[24] Zhu J, Yuan L, Guan Q, Liang G, Gu A. A novel strategy of fabricating high performance UV-resistant aramid fibers with simultaneously improved surface activity, thermal and mechanical properties through building polydopamine and graphene oxide bi-layer coatings. Chem Eng J 2017;310:134–47. https://doi.org/10.1016/j.cej.2016.10.099.

[25] Karakassides A, Ganguly A, Tsirka K, Paipetis AS, Papakonstantinou P. Radially Grown Graphene Nanoflakes on Carbon Fibers as Reinforcing Interface for Polymer Composites. ACS Appl Nano Mater 2020;3:2402–13. https://doi.org/10.1021/acsanm.9b02536.

[26] Han W, Zhou J, Shi Q. Research progress on enhancement mechanism and mechanical properties of FRP composites reinforced with graphene and carbon nanotubes. Alexandria Eng J 2022;64:541–79. https://doi.org/10.1016/j.aej.2022.09.019.

[27] Yandrapu S, Gangineni PK, Ramamoorthy SK, Ray BC, Prusty RK. Effects of electrophoretic deposition process parameters on the mechanical properties of graphene carboxyl-grafted carbon fiber reinforced polymer composite. J Appl Polym Sci 2020;137:1–11. https://doi.org/10.1002/app.48925.

[28] Chen X, Feng Y, Ma Y, Peng S. A facile cathodic electrophoretic deposition (EPD) of GO nanosheet with an orderly layered nanostructure for development of long-term durability anticorrosive coating. Prog Org Coatings 2021;151:106034. https://doi.org/10.1016/j.porgcoat.2020.106034.

[29] Yang J, Yan X, Chen J, Ma H, Sun D, Xue Q. Comparison between metal ion and polyelectrolyte functionalization for electrophoretic deposition of graphene nanosheet films. RSC Adv 2012;2:9665–70. https://doi.org/10.1039/c2ra20948a.

[30] Choi H, Kim H, Hwang S, Han Y, Jeon M. Graphene counter electrodes for dye-sensitized solar cells prepared by electrophoretic deposition. J Mater Chem 2011;21:7548–51. https://doi.org/10.1039/c1jm11145k.

[31] Shen B, Hong H, Chen S, Chen X, Zhang Z. Cathodic electrophoretic deposition of magnesium nitrate modified graphene coating as a macro-scale solid lubricant. Carbon N Y 2019;145:297–310. https://doi.org/10.1016/j.carbon.2019.01.046.

[32] Yu W, Sisi L, Haiyan Y, Jie L. Progress in the functional modification of graphene/graphene oxide: A review. RSC Adv 2020;10:15328–45. https://doi.org/10.1039/d0ra01068e.

[33] Gangineni PK, Yandrapu S, Ghosh SK, Anand A, Prusty RK, Ray BC. Mechanical behavior of Graphene decorated carbon fiber reinforced polymer composites: An assessment of the influence of functional groups. Compos Part A Appl Sci Manuf 2019;122:36–44. https://doi.org/10.1016/j.compositesa.2019.04.017.

[34] Adak NC, Chhetri S, Murmu NC, Samanta P, Kuila T, Lee JH. Experimental and numerical investigation on the mechanical characteristics of polyethylenimine functionalized graphene oxide incorporated woven carbon fibre/epoxy composites. Compos Part B Eng 2019;156:240–51. https://doi.org/10.1016/j.compositesb.2018.08.086.

[35] Kudin KN, Ozbas B, Schniepp HC, Prud'homme RK, Aksay IA, Car R. Raman spectra of graphite oxide and functionalized graphene sheets. Nano Lett 2008;8:36–41. https://doi.org/10.1021/nl071822y.

[36] Malard LM, Pimenta MA, Dresselhaus G, Dresselhaus MS. Raman spectroscopy in graphene. Phys Rep 2009;473:51–87. https://doi.org/10.1016/j.physrep.2009.02.003.

[37] Diba M, Fam DWH, Boccaccini AR, Shaffer MSP. Electrophoretic deposition of graphene-related materials: A review of the fundamentals. Prog Mater Sci 2016;82:83–117. https://doi.org/10.1016/j.pmatsci.2016.03.002.

[38] Das TK, Ghosh P, Das NC. Preparation, development, outcomes, and application versatility of carbon fiber-based polymer composites: a review. Adv Compos Hybrid Mater 2019;2:214–33. https://doi.org/10.1007/s42114-018-0072-z.

[39] Mehdikhani M, Gorbatikh L, Verpoest I, Lomov S V. Voids in fiber-reinforced polymer composites: A review on their formation, characteristics, and effects on mechanical performance. J Compos Mater 2019;53:1579–669. https://doi.org/10.1177/0021998318772152.